

# Photoproduction of $\eta\pi$ pairs off nucleons and deuterons

A. Käser<sup>1</sup>, F. Müller<sup>1</sup>, J. Ahrens<sup>2</sup>, J.R.M. Annand<sup>3</sup>, H.J. Arends<sup>2</sup>, K. Bantawa<sup>4</sup>, P.A. Bartolome<sup>2</sup>, R. Beck<sup>2,5</sup>, A. Braghieri<sup>6</sup>, W.J. Briscoe<sup>7</sup>, S. Cherepnya<sup>8</sup>, S. Costanza<sup>6</sup>, M. Dieterle<sup>1</sup>, E.J. Downie<sup>2,3,7</sup>, P. Drexler<sup>9</sup>, L.V. Fil'kov<sup>8</sup>, A. Fix<sup>10</sup>, S. Garni<sup>1</sup>, D.I. Glazier<sup>3,11</sup>, D. Hamilton<sup>3</sup>, D. Hornidge<sup>12</sup>, D. Howdle<sup>3</sup>, G.M. Huber<sup>13</sup>, I. Jaegle<sup>1</sup>, T.C. Jude<sup>11</sup>, V.L. Kashevarov<sup>2,8</sup>, I. Keshelashvili<sup>1a</sup>, R. Kondratiev<sup>14</sup>, M. Korolija<sup>15</sup>, B. Krusche<sup>1</sup>, V. Lisin<sup>14</sup>, K. Livingston<sup>3</sup>, I.J.D. MacGregor<sup>3</sup>, Y. Maghrbi<sup>1</sup>, J. Mancell<sup>3</sup>, D.M. Manley<sup>4</sup>, Z. Marinides<sup>7</sup>, J.C. McGeorge<sup>3</sup>, E. McNicoll<sup>3</sup>, D. Mekterovic<sup>15</sup>, V. Metag<sup>9</sup>, S. Micanovic<sup>15</sup>, D.G. Middleton<sup>12</sup>, A. Mushkarenkov<sup>6</sup>, A. Nikolaev<sup>2,5</sup>, R. Novotny<sup>9</sup>, M. Oberle<sup>1</sup>, M. Ostrick<sup>2</sup>, P. Otte<sup>2</sup>, B. Oussena<sup>2,7</sup>, P. Pedroni<sup>6</sup>, F. Pheron<sup>1</sup>, A. Polonski<sup>14</sup>, S. Prakhov<sup>16</sup>, J. Robinson<sup>3</sup>, T. Rostomyan<sup>1</sup>, S. Schumann<sup>2,5</sup>, M.H. Sikora<sup>11</sup>, D. Sober<sup>17</sup>, A. Starostin<sup>16</sup>, Th. Strub<sup>1</sup>, I. Supek<sup>15</sup>, M. Thiel<sup>9</sup>, A. Thomas<sup>2</sup>, M. Unverzagt<sup>2,5</sup>, N.K. Walford<sup>1</sup>, D.P. Watts<sup>11</sup>, D. Werthmüller<sup>1,3</sup>, L. Witthauer<sup>1</sup>  
(The A2 Collaboration)

<sup>1</sup> Department of Physics, University of Basel, CH-4056 Basel, Switzerland

<sup>2</sup> Institut für Kernphysik, University of Mainz, D-55099 Mainz, Germany

<sup>3</sup> SUPA School of Physics and Astronomy, University of Glasgow, G12 8QQ, UK

<sup>4</sup> Kent State University, Kent, Ohio 44242, USA

<sup>5</sup> Helmholtz-Institut für Strahlen- und Kernphysik, University Bonn, D-53115 Bonn, Germany

<sup>6</sup> INFN Sezione di Pavia, I-27100 Pavia, Pavia, Italy

<sup>7</sup> Center for Nuclear Studies, The George Washington University, Washington, DC 20052, USA

<sup>8</sup> Lebedev Physical Institute, RU-119991 Moscow, Russia

<sup>9</sup> II. Physikalisches Institut, University of Giessen, D-35392 Giessen, Germany

<sup>10</sup> Laboratory of Mathematical Physics, Tomsk Polytechnic University, Tomsk, Russia

<sup>11</sup> SUPA School of Physics, University of Edinburgh, Edinburgh EH9 3JZ, UK

<sup>12</sup> Mount Allison University, Sackville, New Brunswick E4L3B5, Canada

<sup>13</sup> University of Regina, Regina, SK S4S-0A2 Canada

<sup>14</sup> Institute for Nuclear Research, RU-125047 Moscow, Russia

<sup>15</sup> Rudjer Boskovic Institute, HR-10000 Zagreb, Croatia

<sup>16</sup> University of California Los Angeles, Los Angeles, California 90095-1547, USA

<sup>17</sup> The Catholic University of America, Washington, DC 20064, USA

the date of receipt and acceptance should be inserted later

**Abstract.** Quasi-free photoproduction of  $\pi\eta$ -pairs has been investigated from threshold up to incident photon energies of 1.4 GeV, respectively up to photon-nucleon invariant masses up to 1.9 GeV. Total cross sections, angular distributions, invariant-mass distributions of the  $\pi\eta$  and meson-nucleon pairs, and beam-helicity asymmetries have been measured for the reactions  $\gamma p \rightarrow p\pi^0\eta$ ,  $\gamma n \rightarrow n\pi^0\eta$ ,  $\gamma p \rightarrow n\pi^+\eta$ , and  $\gamma n \rightarrow p\pi^-\eta$  from nucleons bound inside the deuteron. For the  $\gamma p$  initial state data for free protons have also been analyzed. Finally, the total cross sections for quasi-free production of  $\pi^0\eta$  pairs from nucleons bound in  $^3\text{He}$  nuclei have been investigated in view of final state interaction (FSI) effects. The experiments were performed at the tagged photon beam facility of the Mainz MAMI accelerator using an almost  $4\pi$  covering electromagnetic calorimeter composed of the Crystal Ball and TAPS detectors. The shapes of all differential cross section data and the asymmetries are very similar for protons and neutrons and agree with the conjecture that the reactions are dominated by the sequential  $\Delta^*3/2^- \rightarrow \eta\Delta(1232) \rightarrow \pi\eta N$  decay chain, mainly with  $\Delta(1700)3/2^-$  and  $\Delta(1940)3/2^-$ . The ratios of the magnitude of the total cross sections also agree with this assumption. However, the absolute magnitudes of the cross sections are reduced by FSI effects with respect to free proton data.

**PACS.** 13.60.Le Meson production – 14.20.Gk Baryon resonances with S=0 – 25.20.Lj Photoproduction reactions

<sup>a</sup> present address: Institut für Kernphysik, Forschungszentrum Jülich, 52425 Jülich, Germany

Correspondence to: B. Krusche, Klingelbergstrasse 82, CH-4056 Basel, Switzerland, e-mail: Bernd.Krusche@unibas.ch

## 1 Introduction

Photoproduction of meson pairs becomes increasingly important for the study of the electromagnetic excitation spectrum of the nucleon. The reason is simple: so far, many states predicted by quark models have not been observed in experiment. But if one compares the history in nuclear spectroscopy with the situation in hadron spectroscopy, this is not at all surprising. Many features in nuclear structure physics (e.g. rotational and vibrational bands and the like) had not been discovered when only decays of excited states to the nuclear ground states had been investigated. However, this was state of the art in hadron physics until recently. Most experimental efforts were directed to single meson photoproduction ( $\pi$ ,  $\eta$ ,  $\eta'$ ,  $\omega$ ,  $\rho$ ,  $\Phi$ ,...), which corresponds to excited state - ground-state transitions. Production of meson pairs is an important step to more complicated decay mechanisms involving at least one intermediate excited state of the nucleon. Such sequential decays are more probable for higher lying states for which reaction phase space no longer suppresses decays to the  $\Delta$  resonance or to the second resonance region with respect to ground-state decays. This is not the only reason for their importance; one must also consider the hadron structure aspects. In the quark model, high lying states may have both possible oscillator modes excited. For such states, it is a reasonable conjecture that they tend to decay in a two-step process via an intermediate state. The intermediate state could be selected such that in the first transition only one oscillator mode is de-excited followed by a ground-state transition, which de-excites the second one. It would be difficult to identify states with such decay patterns in single meson production reactions and this could suppress entire multiplets of states in the experimental data base.

The study of multiple-meson final states is challenging. The reaction amplitudes for photoproduction of single pseudo-scalar mesons can be fixed by the measurement of at least eight carefully chosen observables [1] as a function of two independent kinematic variables. However, for pseudo-scalar meson pairs [2] the determination of the magnitude of the amplitudes already requires the measurement of eight observables as a function of five kinematic parameters. An extraction of the phases involves the measurement of at least 15 observables. Therefore, ‘complete experiments’, which are currently being discussed for single meson production, are unrealistic. Nevertheless, recent experimental progress is encouraging. The systematic investigation of multiple-meson final states became possible due to the almost  $4\pi$  solid-angle coverage of modern detector systems. In particular, large-angle electromagnetic calorimeters, which can identify recoil nucleons, charged pions, and photons from the decays of neutral mesons, gave a large boost to this program.

The best studied multiple-meson final state is the production of pion pairs, in particular  $\pi^0$  pairs. Reactions with charged mesons are more affected by non-resonant production processes because the photons can directly couple to the charge of the mesons. Nevertheless, such reactions must also be studied in order to reveal the isospin

structure of the excitations. Recently, many new precise experimental results accompanied by detailed reaction analyses became available for pion pairs [3, 4, 5, 6, 7, 8, 9, 10, 11, 12, 13].

The  $\eta\pi$  final state has also attracted interest. Total cross sections, invariant mass distributions, and some polarization observables, have been measured for the production of  $\eta\pi^0$  pairs off protons at LNS in Sendai, Japan [14], GRAAL at ESRF in Grenoble, France [15], ELSA in Bonn, Germany [16, 17, 18, 19, 20], and at MAMI in Mainz, Germany [21, 22] (see [25] for a recent summary). In comparison to pion pairs, this channel has more selectivity. As far as decays of nucleon resonances are concerned the iso-scalar  $\eta$  meson can only be emitted in transitions between two  $N^{(*)}$  or between two  $\Delta^{(*)}$  states (but not in  $N^{(*)} \leftrightarrow \Delta^{(*)}$  transitions). The  $\Delta$ -like resonances decay into  $N\eta\pi$  mainly via two sequences,  $\Delta^* \rightarrow \eta\Delta(1232)3/2^+$  and  $\Delta^* \rightarrow \pi N(1535)1/2^-$ , whereas the  $N^*$  states produce the final  $N\eta\pi$  state only by pion emission to the  $\pi N(1535)1/2^-$  channel. Therefore, the reaction is in particular sensitive to excited resonances, whose decay via the first sequence  $\Delta^* \rightarrow \eta\Delta(1232)3/2^+$  leaves its trace in the  $\pi N$  invariant mass spectra, peaking at  $\Delta(1232)$ . The  $\Delta^*(N^*) \rightarrow \pi N(1535)1/2^- \rightarrow N\pi\eta$  transitions produce  $\eta$ -nucleon invariant masses  $m(\eta, N)$  characteristic for the  $N(1535)1/2^-$  state (i.e. close to the kinematical lower limit of  $m(\eta, N)=1485$  MeV). At sufficiently large incident photon energies, contributions from the  $a_0(980)$  meson are expected. Its decay to  $\eta\pi$  results in a peak in the  $\eta$ -pion invariant mass spectrum [16, 17, 20].

The analysis of the available data for the  $\gamma p \rightarrow p\pi^0\eta$  reaction, including invariant mass distributions, angular distributions, and polarization observables measured with circularly and linearly polarized photon beams [17, 20, 21, 22, 23], has revealed a strong contribution of the  $\Delta(1700)3/2^- \rightarrow \eta\Delta(1232) \rightarrow \eta\pi^0 p$  decay chain in the threshold region. In [21], the authors have shown that with the contribution of the  $\Delta(1700)3/2^-$  alone (no background terms, no further nucleon resonances), most features of the total cross section and several types of angular distributions can be described. With the availability of experimental results for polarization observables (beam-helicity asymmetry in [22] and beam asymmetry in [15, 18]), the model was extended in [23] to contributions from several  $I = 3/2$   $\Delta$ -resonances and background terms (Born-terms). Predictions for further polarization observables from the extended model have been made in [24]. Using data from the CBELSA/TAPS experiment, which cover a larger energy range and provide polarization observables measured with linearly polarized photon beams, the reaction has also been analyzed in the framework of the Bonn-Gatchina coupled channel model [20]. So far, all results are consistent with a dominant contribution from the  $\Delta(1700)3/2^-$  resonance in the threshold region. Therefore, this reaction is promising for a detailed investigation of this state, which is interesting because its nature is not yet well established. Besides the interpretation as a standard three-constituent-quark state, a dynamical generation within

coupled-channel chiral unitary theory for meson-baryon scattering has also been discussed [26, 27].

So far, data are only available for the  $\gamma p \rightarrow p\pi^0\eta$  reaction. However, the isospin dependence of the production of  $\pi\eta$  pairs is also of great interest. Since the  $\eta$ -meson is isoscalar, the isospin structure of the  $\pi\eta$  photoproduction amplitude is identical to that for single  $\pi$  photoproduction. Its different charge channels may be represented as:

$$\begin{aligned} A(\gamma p \rightarrow n\pi^+\eta) &= -\sqrt{\frac{1}{3}} A^{V3} + \sqrt{\frac{2}{3}}(A^{IV} - A^{IS}) \quad (1) \\ A(\gamma p \rightarrow p\pi^0\eta) &= +\sqrt{\frac{2}{3}} A^{V3} + \sqrt{\frac{1}{3}}(A^{IV} - A^{IS}) \\ A(\gamma n \rightarrow p\pi^-\eta) &= +\sqrt{\frac{1}{3}} A^{V3} - \sqrt{\frac{2}{3}}(A^{IV} + A^{IS}) \\ A(\gamma n \rightarrow n\pi^0\eta) &= +\sqrt{\frac{2}{3}} A^{V3} + \sqrt{\frac{1}{3}}(A^{IV} + A^{IS}). \end{aligned}$$

where  $A^{IS}$  is the isoscalar matrix element,  $A^{IV}$  is the isovector, and  $A^{V3}$  is the isospin changing one. Only the latter contributes to the excitation of  $\Delta$  states.

From the decomposition of Eq. 1, one easily sees that for the reaction chain  $\gamma N \rightarrow \Delta^* \rightarrow N\pi\eta$  ( $A^{IS}, A^{IV} = 0$ ), the cross section ratios for production of neutral and charged pions off protons and neutrons are related by:

$$\begin{aligned} \sigma(\gamma p \rightarrow \eta\pi^0 p) &= \sigma(\gamma n \rightarrow \eta\pi^0 n) = \\ 2\sigma(\gamma p \rightarrow \eta\pi^+ n) &= 2\sigma(\gamma n \rightarrow \eta\pi^- p). \end{aligned} \quad (2)$$

Any deviations from this relation would signal contributions from  $I = 1/2$   $N^*$  resonances or from non-resonant background. In the present work, all four isospin channels have been studied using liquid hydrogen and liquid deuterium targets. The total cross sections and their ratios already have been published in a preceding letter [28]. The present paper summarizes the results for differential cross sections (invariant mass distributions of the meson - meson and meson - nucleon pairs and angular distributions), as well as the results for the helicity asymmetry  $I^\odot$ , which was measured with a circularly polarized photon beam and an unpolarized target.

## 2 Definition of observables

All differential cross sections presented in this paper were normalized to the respective total cross sections in order to facilitate the comparison of different reaction channels and between experimental results and model predictions. A kinematic reconstruction of the final state (as described in [29]) was used to determine the photon - nucleon center-of-momentum (cm) energy  $W$ , the kinetic energy of the recoil nucleon, and all relevant cm angles (see Sec. 4). It uses as input the incident photon energy and the measured four momenta of the pions and  $\eta$  mesons and the polar and azimuthal angles of the detected recoil nucleons. The effects from nuclear Fermi motion were thus removed. Due to the small total cross sections (maximum values around  $2.5 \mu b$

for  $\pi^0$  mesons and around  $1.5 \mu b$  for charged mesons), the statistical quality of the data was only sufficient to separate the total range of photon - nucleon invariant mass from  $W=1.7 - 1.9$  GeV into four bins.

The first group of experimental data comprises the invariant mass distributions of meson - meson and meson - nucleon pairs. Their definition as the magnitude of the sum of the four momenta of the particle pairs is straightforward. Previous results are only available for the  $\pi^0\eta$  final state for free protons (see [20] and Refs. therein).

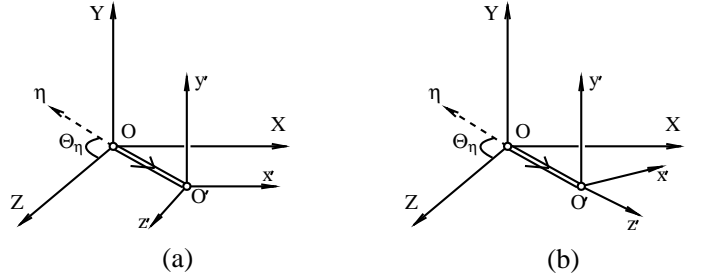


**Fig. 1.** Definition of coordinate frames for angular distributions in the nucleon - pion rest frames for (a) the canonical system, and (b) the helicity system [21]. In the canonical system (a) the  $z'$  axis is parallel to the photon beam direction, in the helicity system (b), it is in direction of the combined  $\pi N$  momentum (thick arrow). The  $x'$  axis is in the reaction plane in both systems and the  $y'$  axis is perpendicular to this plane.

Angular distributions have been analyzed in the same way as in [21, 23], which is adapted to the hypothesis of a dominant  $\Delta^* \rightarrow \Delta(1232)\eta \rightarrow \eta\pi N$  decay. The axes of the photon - nucleon cm system are denoted by  $X, Y, Z$  (the photon is in the direction of the  $Z$  axis and the incident nucleon is in the  $-Z$  direction). Note that the  $Z$  direction is not necessarily parallel to the laboratory beam axis because the incident nucleon may have a momentum in a different direction due to Fermi motion. The momenta of the  $\eta$  meson and the combined  $\pi N$  system are back-to-back in this overall cm frame. Angular distributions of the pions in the pion - nucleon cm system have been extracted in two different frames, as shown in Fig. 1. In the canonical frame, the  $z'$ -axis is parallel to the photon direction, while in the helicity frame, it is in direction of the momentum of the combined  $N\pi$  system, i.e. in the direction of the momentum vector of the supposed intermediate  $\Delta(1232)$  resonance. The direction of the  $y'$  axes are for both frames chosen as:

$$\hat{y}' = (\mathbf{p}_\eta \times \mathbf{k}_\gamma) / |\mathbf{p}_\eta \times \mathbf{k}_\gamma| \quad (3)$$

and the  $x'$  axes lie in both systems in the reaction plane and are oriented such that a right handed coordinate frame results. Angular distributions were constructed for the polar angle  $\Theta_\eta$  of the  $\eta$ -meson in the photon - nucleon overall cm frame and for the polar ( $\Theta_c, \Theta_h$ ) and azimuthal ( $\Phi_c, \Phi_h$ ) angles of the pion in the canonical ('c') and helicity ('h') frames. Previous results for such angular distributions for photoproduction of  $\pi^0\eta$  pairs off free protons are given in [21].

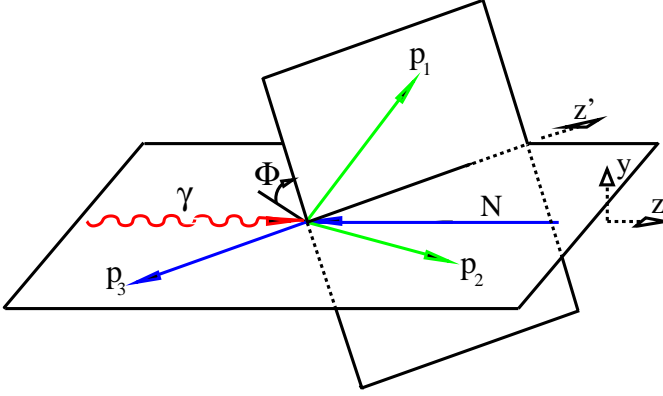


**Fig. 2.** Vector and angle definitions in the cm system of incident photon ( $\gamma$ ) and initial-state participant nucleon  $N$ . Particles  $p_1$ ,  $p_2$ , and  $p_3$  are some permutation of the final-state participant nucleon  $N'$ , the pion, and the  $\eta$  meson, depending on the type of the asymmetry (see text). One plane is defined by the momentum of the incident photon  $\mathbf{k}$  and the momentum of particle  $p_3$ , the other by the momenta of particles  $p_1$  and  $p_2$  (all momenta in the photon - nucleon cm system).  $\Phi$  is the angle between the planes.

Final states with three particles (such as  $\pi\pi N$  or  $\pi\eta N$ ) can show an asymmetry, the beam-helicity asymmetry  $I^\circ$ , even when investigated with an unpolarized target and a circularly polarized photon beam. The definition of the asymmetry is shown in Fig. 2. Two planes are defined in the photon-nucleon cm system by the three final-state particles and the incident photon (or nucleon). The asymmetry due to the photon beam helicity can be defined as a function of the angle  $\Phi$  between the two planes by:

$$I^\circ(\Phi) = \frac{d\sigma^+ - d\sigma^-}{d\sigma^+ + d\sigma^-} = \frac{1}{P_\gamma} \frac{N^+ - N^-}{N^+ + N^-}, \quad (4)$$

where  $d\sigma^\pm$  are the differential cross sections for each of the two photon helicity states,  $P_\gamma$  is the degree of circular polarization of the photons, and  $N^\pm$  are the count rates for the two helicity states. The integration of the count rates over extended phase-space regions has to be corrected for detection efficiency effects. In the present analysis, results are presented for the choices  $(p_1, p_2, p_3) = (\eta, \pi, N)$ ,  $(\pi, N, \eta)$ , and  $(\eta, N, \pi)$ . The corresponding angles are labeled  $\Phi_1$ ,  $\Phi_2$ , and  $\Phi_3$  and the asymmetries are denoted as  $I^\circ(\eta, \pi, N)$ ,  $I^\circ(\pi, N, \eta)$ , and  $I^\circ(\eta, N, \pi)$ . Previous results for  $I^\circ(\pi, N, \eta)$  for  $\pi^0\eta$  pairs produced on free protons are given in [22].

Due to parity conservation, all asymmetries must obey the condition:

$$I^\circ(\Phi) = -I^\circ(2\pi - \Phi), \quad (5)$$

and can be expanded into sine series:

$$I^\circ(\Phi) = \sum_{n=1}^{\infty} A_n \sin(n\Phi) \quad (6)$$

which can be fitted to the data. Test fits produced no  $A_i$ ,  $i \geq 3$  results significantly different from zero. This was

due to the limited statistical precision. Therefore, the final fits were restricted to the  $A_1$  and  $A_2$  coefficients.

### 3 Experimental setup

The experimental setup and all relevant parameters have already been discussed in detail in several publications (see [8, 9, 13, 28, 30, 31, 32] for the measurements with deuterium targets and [33, 34] for the  $^3\text{He}$  data), which used the same data sets. Therefore, only a short summary is given here. The experiments were carried out at the Mainz MAMI accelerator [35, 36] using a quasi-monochromatic photon beam with energies up to  $\approx 1.4$  GeV from the Glasgow tagged photon spectrometer [37, 38, 39]. The electrons were longitudinally polarized and this polarization is transferred in the bremsstrahlung process to circular polarization of the photons. The degree of circular polarization of the photon beam is energy dependent and is related to the degree of linear polarization of the electron beam by the transfer function given by Olsen and Maximon in [40]. The polarization degree of the electron beam was measured by Mott and Møller scattering (typical values were in the range 60 - 85%, see [8, 9]).

In total, results from three different beam times with liquid deuterium targets, one beam time with a liquid hydrogen target, and one beam time with a liquid  $^3\text{He}$  target, were analyzed for the present results. Their main parameters are listed in Table 1. The target cells were Kapton cylinders (a Mylar cylinder for the liquid  $^3\text{He}$ ) of  $\approx 4$  cm diameter. Target lengths, densities, and the beam parameters of the different beam times are summarized in Table 1.

**Table 1.** Summary of data samples. Target type ( $LD_2$ : liquid deuterium,  $LH_2$ : liquid hydrogen,  $L^3He$ : liquid  $^3\text{He}$ ), target length  $d$  [cm], target surface density  $\rho_s$  [nuclei/barn], electron beam energy  $E_{e^-}$  [MeV], degree of longitudinal polarization of the electron beam  $P_{e^-}$  [%].

Target	$d$ [cm]	$\rho_s$ [barn $^{-1}$ ]	$E_{e^-}$ [MeV]	$P_{e^-}$ [%]
$LD_2$	4.72	$0.231 \pm 0.005$	1508	$61 \pm 4$
$LD_2$	4.72	$0.231 \pm 0.005$	1508	$84.5 \pm 6$
$LD_2$	3.00	$0.147 \pm 0.003$	1557	$75.5 \pm 4$
$LH_2$	10.0	$0.422 \pm 0.008$	1557	$75.5 \pm 4$
$L^3He$	5.08	$0.073 \pm 0.005$	1508	-

Recoil nucleons, charged pions, and photons from the decay of the neutral mesons were detected in an almost  $4\pi$  solid angle electromagnetic calorimeter, supplemented with detectors for charged particle identification (see Fig. 3). The main components of this setup were the Crystal Ball (CB) detector [43] comprising 672 NaI crystals and a hexagonal forward wall constructed from 384 BaF<sub>2</sub> modules of the TAPS device [41, 42]. The CB covered polar angles from  $20^\circ$  to  $160^\circ$  and the TAPS forward wall covered polar angles down to  $\approx 5^\circ$ . All TAPS modules were equipped with individual plastic scintillators for charged

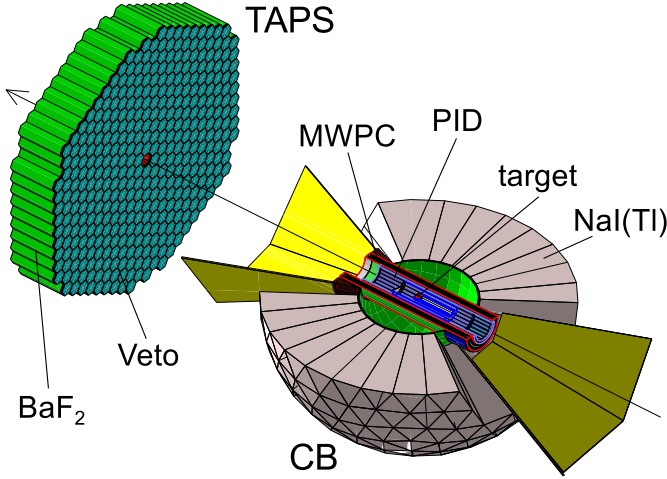


**Fig. 3.** Setup of the electromagnetic calorimeter combining the Crystal Ball and TAPS (left hand side) detectors. Only the lower half-shell of the Crystal Ball detector is shown. Detectors for charged particle identification are mounted in the Crystal Ball (PID and MWPC) and in front of the TAPS forward wall (TAPS Veto-detector).

particle identification in front of the crystals. The target was placed in the center of the CB and surrounded by a detector for charged particle identification (PID) [44].

## 4 Data analysis

The data analysis for the final states summarized in this paper has already been discussed in [28], where the total cross sections were presented. More details have been given for the almost identical analyses of the  $N\pi^0\pi^0$  and  $N\pi^0\pi^\pm$  final states [9,13] from the same data set. Therefore, only a brief summary is given here.

In the first step of the analysis, the charged particle detectors in front of TAPS and inside the CB were used to classify the hits in the calorimeters as ‘charged’ or ‘neutral’. Subsequently, a  $E - \Delta E$  analysis, comparing the energy deposition in the PID to the full energy of the particle measured with the CB was used to separate protons and charged pions (see Fig. 4, left hand side). Charged pions in TAPS were not analyzed because the contamination with the more abundant protons was substantial. This means that a small part of the reaction phase space (charged pions at polar angles smaller than  $20^\circ$ ) was excluded from the analysis (this was taken into account for the simulation of the detector acceptance and efficiency). Recoil protons and neutrons in TAPS were identified with a time-of-flight versus energy and a pulse-shape analysis.

The events characterized in Table 2 were then accepted for the analysis of (quasi)-free production off protons ( $\sigma_p$ ), off neutrons ( $\sigma_n$ ), and the inclusive reaction off the deuteron ( $\sigma_{\text{incl}}$ ), for which recoil nucleon detection was not required, but allowed. The inclusive cross section has only been used to check the relation:

$$\sigma_{\text{incl}} \approx \sigma_p + \sigma_n + (\sigma_d), \quad (7)$$

**Table 2.** Selected event classes for the cross sections  $\sigma_p$  (coincident with recoil protons),  $\sigma_n$  (coincident with recoil neutrons), and  $\sigma_{\text{incl}}$  (no condition for recoil nucleons) for  $\pi\eta$ -pairs with neutral and charged pions.  $n$  and  $c$  denote neutral and charged hits in the calorimeter (distinguished by the response of the charged-particle detectors).

	$\sigma_p$	$\sigma_n$	$\sigma_{\text{incl}}$
$\pi^0\eta$	$4n\&1c$	$5n$	$4n$ or $5n$ or $(4n\&1c)$
$\pi^\pm\eta$	$2n\&2c$	$3n\&1c$	$(2n\&1c)$ or $(2n\&2c)$ or $(3n\&1c)$

where the (small) coherent cross section  $\sigma_d$  measured in coincidence with recoil deuterons contributes only for  $\pi^0\eta$  pairs. As shown in [28], maximum deviations from Eq. 7 are below 5%, which limits possible uncertainties for the detection of recoil nucleons ( $\sigma_p$ ,  $\sigma_n$ , and  $\sigma_d$  depend on them, but  $\sigma_{\text{incl}}$  does not).

Photons and neutrons cannot be distinguished in the CB (the flight path is too short for time-of-flight versus energy analysis, there is no pulse-shape analysis, and cluster-size distributions of electromagnetic showers and energy depositions from neutrons in the CB do not allow for an event-by-event separation (see [13,28,31])). Therefore, neutral hits were assigned with a  $\chi^2$  analysis to photons and neutrons. For events with three or five neutral hits, the invariant masses of all possible pair combinations were compared to the mass of the  $\pi^0$ , or the  $\pi^0$  and  $\eta$  masses, respectively. For events with  $n_m$  neutral mesons ( $n_m = 1$  for  $\pi^\pm\eta$  final states,  $n_m = 2$  for  $\pi^0\eta$ )  $\chi^2$  was defined by

$$\chi^2(k) = \sum_{i=1}^{n_m} \left( \frac{m_{\pi^0,\eta} - m_{i,k}}{\Delta m_{i,k}} \right)^2 \quad \text{with } k = 1, \dots, n_p, \quad (8)$$

where the  $m_{i,k}$  are the invariant masses of the  $i$ -th pair in the  $k$ -th permutation of the hits and  $\Delta m_{i,k}$  is the corresponding uncertainty computed event-by-event from the experimental energy and angular resolution. In order to suppress combinatorial background, not only the hypotheses of  $\pi^0\eta$  pairs (for events with five neutrals) or  $\eta$  mesons (for events with three neutrals) but also those of  $\pi^0\pi^0$  pairs, or single  $\pi^0$  production were tested. In all cases, only the combination with the minimum  $\chi^2$  was selected for further analysis. A two-dimensional invariant mass spectrum of events with four photons is shown in Fig. 4, (right hand side), and details are discussed in [28].

In the final step of the reaction identification, residual background was removed by an analysis of the coplanarity of the final state particles and the missing mass of the reaction when the recoil nucleon (although detected) was treated as a missing particle (see [28] for details). The coplanarity analysis is based on the fact that in the cm system (apart from Fermi smearing) the momentum vector of the combined  $\pi\eta$  system must be back-to-back with the recoil nucleon momentum, so that the azimuthal angles of the nucleon and the combined  $\eta\pi$  laboratory momentum must differ by  $180^\circ$ . This cut suppresses also the rare events were due to large Fermi momenta the spectator nucleon is detected instead of the participant nucleon. The

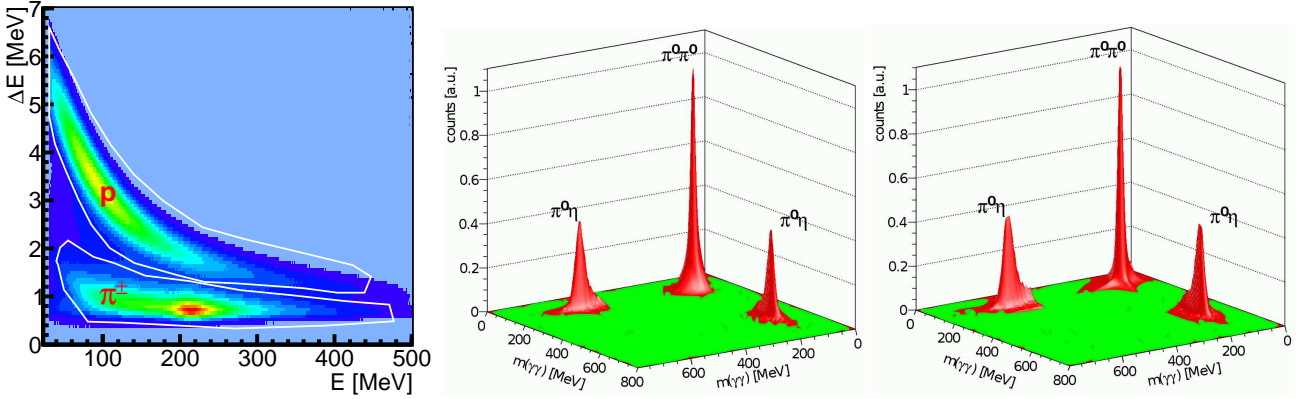


**Fig. 4.** Left hand side [28]: Identification of protons and charged pions in CB with a  $\Delta E$  (energy depositon in PID) versus  $E$  (total energy measured with CB) analysis. White lines indicate the accepted areas. Center (right hand side): two-dimensional invariant-mass distributions for events with four photons in coincidence with recoil protons (recoil neutrons). The regions around the  $\pi^0\eta$  peaks are scaled up by a factor of 50.

missing mass analysis uses the incident photon energy and the four momenta of the two mesons to kinematically reconstruct the mass of the ‘missing’ particle (the detected participant recoil nucleon, Fermi motion is neglected) and compares it to the mass of the nucleon via:

$$\Delta M = |P_\gamma + P_N - P_\pi - P_\eta| - m_N, \quad (9)$$

where  $m_N$  is the nucleon mass,  $P_\gamma$  is the four-momentum of the incident photon,  $P_N$  is the four momentum of the initial state nucleon (assumed at rest), and  $P_\pi$  and  $P_\eta$  are the four momenta of the two mesons. Typical spectra for all four reactions for the energy ranges of interest are summarized in Fig. 5. They are almost background free and the shape of the distributions is in good agreement with Monte Carlo simulations. The tails of the distributions were rejected in order to remove small residual backgrounds and kinematically poorly reconstructed events.

Absolute cross sections were extracted from the measured yields, as described in [28] (more details are given in [13,31] for other reactions), from the target surface densities, the photon flux, the meson decay branching ratios, and the simulated (Geant4 [45]) detection efficiency of the experimental setup. For the asymmetries, the polarization degree of the photon beam also matters, which was discussed in [8,9] in context of the photoproduction of pion pairs.

For the total cross sections, which have been summarized in [28], two different analyses were done. Excitation functions were obtained as a function of the photon energy measured with the tagging spectrometer. This analysis suffered from Fermi smearing. The other analysis reconstructed the final state total energy  $W$  from the incident photon energy, the four momenta of the mesons, and the polar and azimuthal angles of the detected recoil nucleon. This analysis eliminated the effects from Fermi motion, but introduced effects from angular and energy resolution of the calorimeter. For the differential cross sections and asymmetries, only the second method was used because Fermi smearing obscures these observables too

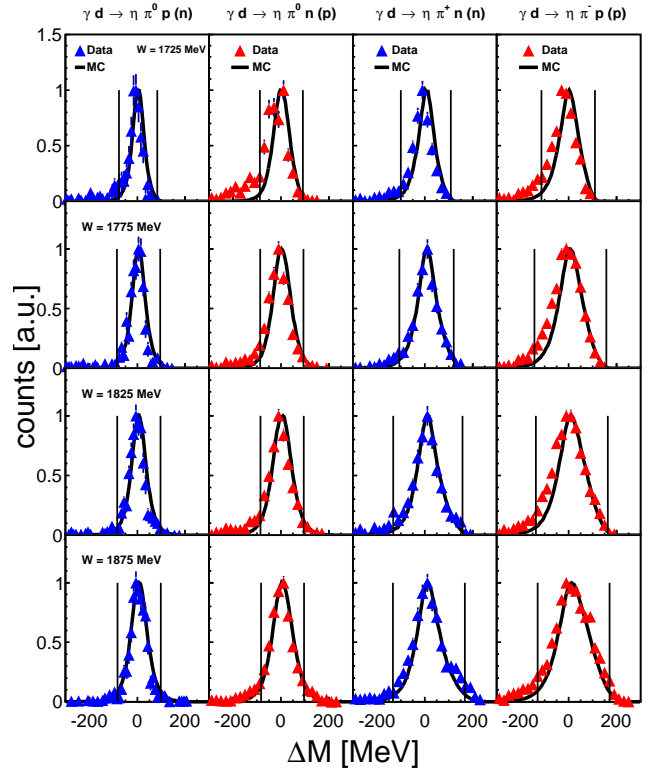


**Fig. 5.** Missing mass distributions. From top to bottom: different values of  $W$  corresponding to the ranges for which differential cross sections and asymmetries were extracted (center values  $\pm 25$  MeV). Columns from left to right: reactions  $\gamma d \rightarrow \eta\pi^0 p(n)$ ,  $\gamma d \rightarrow \eta\pi^0 n(p)$ ,  $\gamma d \rightarrow \eta\pi^+ n(n)$ , and  $\gamma d \rightarrow \eta\pi^- p(p)$  (in parenthesis undetected spectator nucleon). Triangles are data, and solid curves are MC simulation of the signals. Vertical lines: ranges of accepted events.

much. Note that the kinematic reconstruction of the final state is only exact for the deuterium target. For the  $^3\text{He}$  target, it is based on the (fairly good) approximation that



the two spectator nucleons have no relative momentum (for details see [34]).

Systematic uncertainties have been discussed in detail in [8, 9, 13, 31], which analyzed the same data for other reaction channels, and in [28] specifically for the production of  $\pi\eta$  pairs. The total overall normalization uncertainty (photon flux, target density) was estimated to be between 5% (quadratic addition) and 7% (linear addition). Uncertainties from analysis cuts including simulation of the detection efficiency, but excluding the recoil nucleon detection, were in the range of 5 - 10% (larger uncertainties for charged pions). The detection efficiency has been simulated with different event generators using reaction phase space and the  $\Delta^* \rightarrow \eta\Delta(1232) \rightarrow \eta\pi^0 p$  decay chain. The differences were small and the results from the sequential decay, which is in excellent agreement with the measured invariant mass distributions, were used. In addition to Monte Carlo simulations, the recoil nucleon detection efficiencies have been also experimentally investigated with reactions such as  $\gamma p \rightarrow p\eta$ ,  $\gamma p \rightarrow p\pi^0$ ,  $\gamma p \rightarrow p\pi^0\pi^0$  for recoil protons and  $\gamma p \rightarrow n\pi^+\pi^0$  for recoil neutrons [13, 31]. The systematic uncertainty of these analyses has been estimated in [31] at the 10% level, but the good agreement between the sum of the exclusive cross sections and the inclusive results for many different reaction channels suggest that this is an upper limit. Most of the uncertainties cancel in the isospin ratios discussed in [28]. The systematic uncertainty of the asymmetries is dominated by the precision of the measurement of the polarization degree of the electron beam (see Table 1).

## 5 Results

Total cross sections and their ratios for the different isospin channels have already been presented in [28]. Here, the main results are summarized. All differential distributions have been normalized by the absolute scale of the total cross sections for easier comparison of the shapes. Fig. 6 shows the total cross sections for the four final states as a function of the incident photon energy (Figs. 6(a),(b)) and as a function of the final state invariant mass  $W$  (Figs. 6(c),(d)). Only the exclusive quasi-free cross sections measured in coincidence with recoil nucleons are shown and compared to previous and present results for a free proton target. A comparison of the inclusive cross sections to the sum of the exclusive ones was made in Ref. [28] to demonstrate the validity of Eq. 7.

The total cross section for the  $\gamma p \rightarrow p\pi^0\eta$  reaction is in very good agreement with the previous measurement from Ref. [21] (note that the results from CBELSA [20] were originally  $\approx 15\%$  lower, but have been renormalized in [20] to [21] because of their larger systematic uncertainty). For the  $\pi^0\eta$  final state, significant effects from final state interactions (FSI) have been observed. When analyzed as a function of incident photon energy, the quasi-free cross section for production off protons is roughly 75% for protons bound in the deuteron and only 50% for protons bound in  $^3\text{He}$ , both relative to the cross section for the free proton target. Analyzed as a function of final state

$W$ , the quasi-free cross sections are 75% and 60% relative to the free-proton cross section. For the results analyzed as a function of  $E_\gamma$ , deviations between free and quasi-free reactions are due to FSI effects *and* Fermi smearing. Fermi motion effects have been removed from the  $W$  data (some residual effects from the reconstruction may be present in the immediate vicinity of the production threshold, which is, however, not discussed in detail). Since the Fermi motion effects are larger for the  $^3\text{He}$  nucleus, the observed behavior is plausible.

The FSI effects are smaller for the  $\pi^\pm\eta$  final states (cross section for protons bound in the deuteron reduced to  $\approx 90\%$ ; it was not analyzed for the  $^3\text{He}$  target). This behavior is similar to the photoproduction of single pions. Also in this case FSI effects are larger for neutral pions due to the difference between nucleon-nucleon interactions in the  $np$  system (which can be bound) compared to the  $nn$  and  $pp$  systems [47]. However, a quantitative understanding of the FSI effects is not yet available. The comparison of differential spectra discussed below seems to indicate that the FSI effects manifest themselves mainly in the absolute scale of the cross sections.

The ratios of the different isospin channels agree with the expectation for the  $\Delta^* \rightarrow \eta\Delta(1232) \rightarrow \eta\pi^0 p$  decay chain given in Eq. 2. They are summarized in Fig. 6(e). These ratios could be influenced by FSI effects when FSI is different for recoil protons and recoil nucleons and/or for charged and neutral pions. For the  $\pi^0\eta$  final state, the  $\sigma_n/\sigma_p$  ratio (quasi-free nucleons) extracted from the deuterium and  $^3\text{He}$  targets are comparable, although the absolute effect from FSI is much stronger for the helium target. This is an indication that FSI for quasi-free neutrons and protons are similar and thus the quasi-free neutron/proton ratios are a good approximation for the reactions with free nucleons. The situation is different for the comparison of reactions with the same type of target nucleon, but different charge states of the pions since, as discussed above, FSI effects are more significant for production of neutral pions than for charged pions. Fig. 6(e) shows the ratios of neutral/charged pion cross sections as measured (solid symbols) and rescaled by the ratio of FSI effects observed for protons ( $75\% \div 90\% = 0.83$ ) (open symbols). Within uncertainties, the results are in agreement with Eq. 2.

The results with the effects from Fermi motion corrected are compared in Figs. 6(c),(d) to the predictions from [23]. All results from this reference correspond to their fit solution (I), which is in best agreement with data for the  $\gamma p \rightarrow p\pi^0\eta$  reaction (in particular for the beam asymmetry  $\Sigma$ ). This is their basis solution with the strong  $D_{33}$  dominance. Their solution (II) has at high incident photon energies a larger contribution from the  $\Delta(1920)3/2^+$  state and their solution (III) has an admixture of the  $\Delta(1700)3/2^- \rightarrow \Delta(1232)\eta$  decay in  $d$ -wave, which is neglected in solution (I) which assumes only  $s$ -wave decay of this state. The model has not been fitted to the present data, i.e. not to any data with neutrons in the initial state or charged pions in the final state. The model predictions are only valid for free proton and free neutron targets and

do not include FSI effects. Therefore, all differential spectra have been renormalized to the total cross sections so that the major FSI effects were eliminated in the comparison of measured data and predictions.



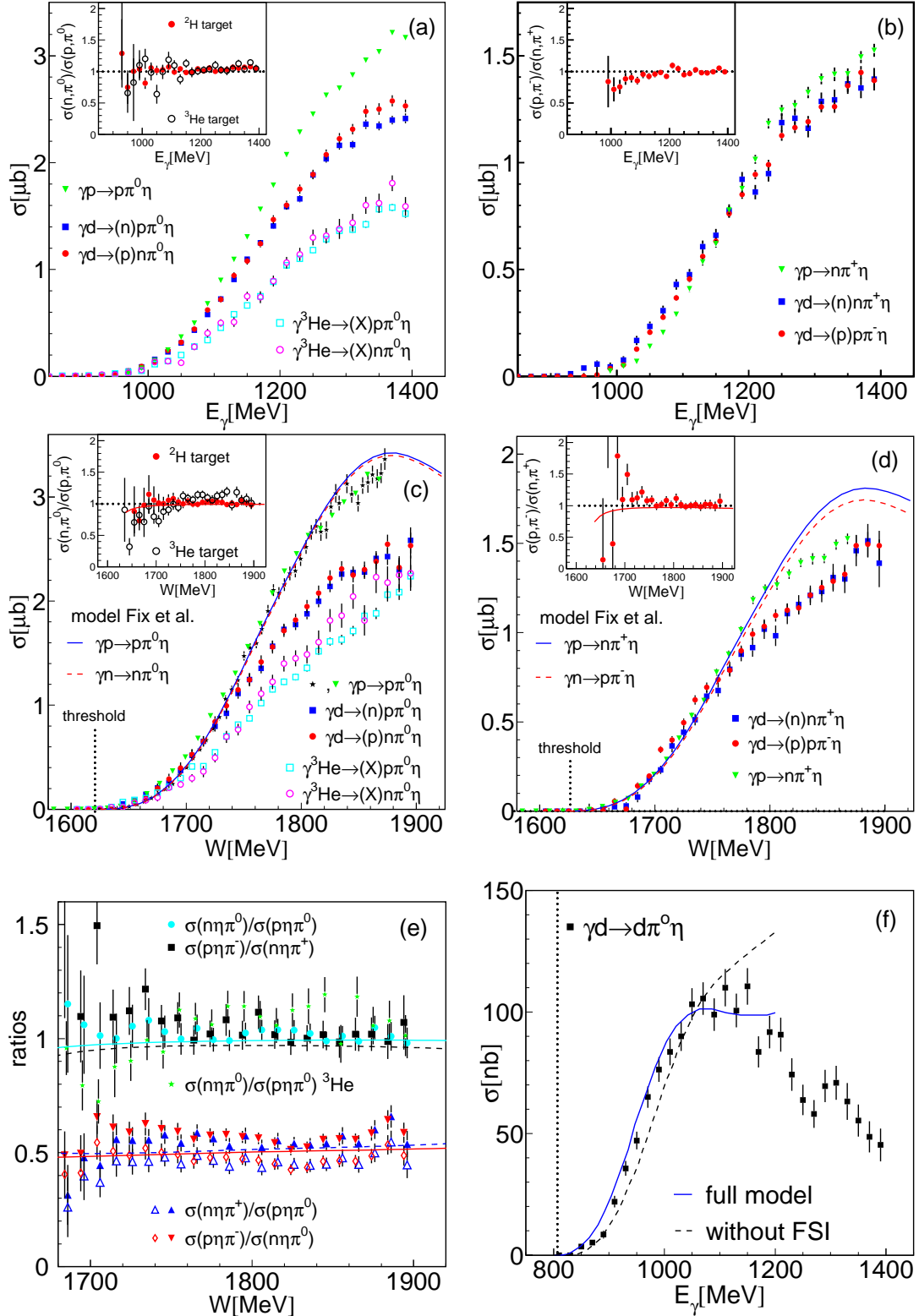


**Fig. 6.** Total cross sections for  $\gamma N \rightarrow N\pi\eta$  reactions. (a) and (b) show the results as a function of photon energy, (c) and (d) as a function of final state invariant mass. Figures on the left hand side ((a) and (c)) correspond to the  $\pi^0\eta$  final state, figures on the right hand side ((b) and (d)) to the  $\pi^\pm\eta$  final state. The different reactions are indicated in the figures. Previous results for  $\gamma p \rightarrow p\pi^0\eta$  in (c), black stars, are from [21]. The inserts show the ratio of quasi-free production off neutrons and protons from deuterium targets and for the  $\pi^0\eta$  final state also for a  $^3\text{He}$  target. (e) summarizes the results for the ratios of the isospin channels. For the ratios involving charged and neutral pions the solid symbols are as measured and the open symbols are re-scaled for FSI effects (see text). The curves represent the model results from [23]. (f) shows the data for the  $\gamma d \rightarrow d\pi^0\eta$  reaction [28] with model results from [46]. Only the statistical uncertainties are shown.

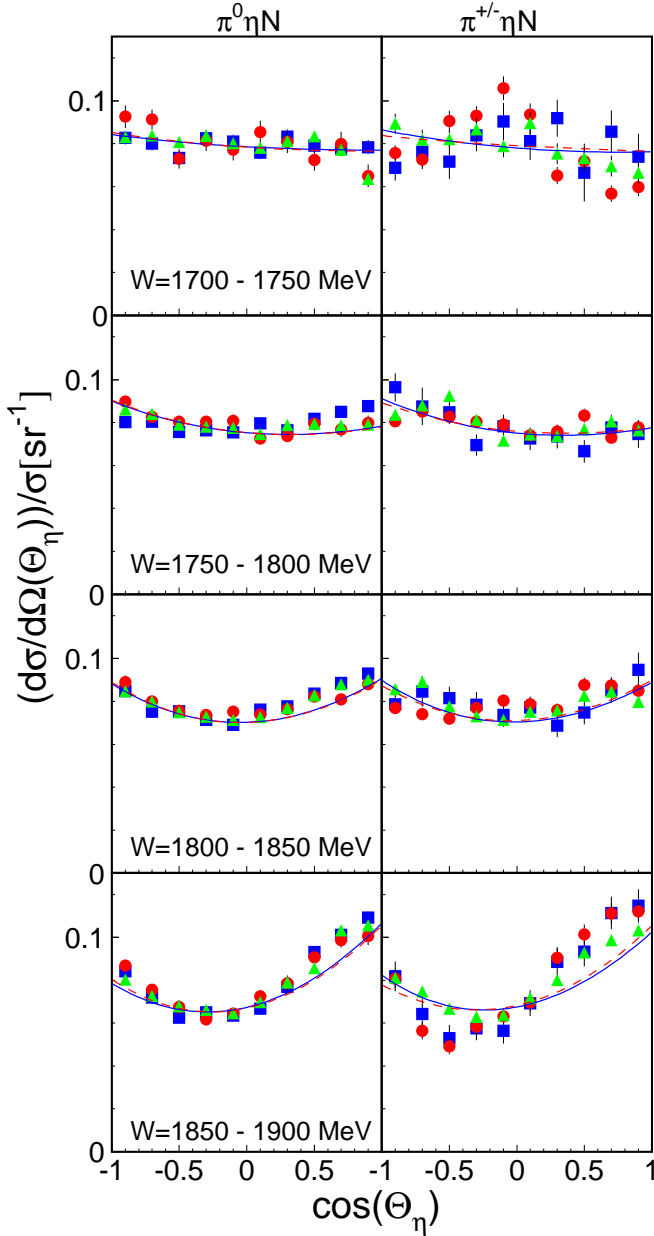


**Fig. 7.** Distributions of the polar angles of the  $\eta$  mesons in the photon - nucleon cm frame. Left hand side: neutral pions, right hand side: charged pions. Ranges for invariant mass  $W$  are given in the figure. Initial states: (green) triangles: free protons, (blue) squares quasi-free protons and (red) circles: quasi-free neutrons. Curves for model results from [23], solid (blue) for target protons, dashed (red) target neutrons (proton and neutron predictions are almost identical).

The model predicts similar results for protons and neutrons for the total magnitude of the cross sections. The differences for charged pions are slightly larger than for neutral pions but still below the 4% level for all values of  $W$ . The predictions for the shape of the differential distributions for protons and neutrons are even closer to each other, as discussed below.

This is inherent to the model assumptions because in the initial electromagnetic photon-excitation process  $\gamma N \rightarrow R$ , only  $I = 3/2$   $\Delta$  resonances are taken into account for  $R$  (with subsequent hadronic decay to  $\Delta\eta$  or  $N^*\pi$  intermediate states). Isospin  $I = 1/2$  components contribute only via non-resonant background terms (Born-diagrams). Since the  $\gamma N \Delta$  couplings are equal for protons and neutrons, the predicted proton and neutron cross sections from resonance excitations are identical.

The effects of the Born-terms are minor such that for the renormalized differential spectra in most figures, model results for proton and neutron targets are indistinguishable. Apart from small differences for the contributions of the Born-terms to reactions with neutral and charged pions, the relation between cross sections for different pion types is simply given by the Clebsch-Gordon coefficients. For the ratios of the total cross sections (for which the dominant FSI effects cancel), these predictions are clearly supported by the experimental results (see Figs. 6 (c)-(e)).

Also analyzed [28] was the coherent production of  $\eta\pi^0$  pairs off the deuteron:

$$\gamma + d \rightarrow d + \eta + \pi^0. \quad (10)$$

Since the deuteron has isospin  $I = 0$ , the amplitude of this reaction is proportional to the sum of the amplitudes on protons and neutrons:

$$A(\gamma d \rightarrow d\pi^0\eta) \propto A(\gamma p \rightarrow p\pi^0\eta) + A(\gamma n \rightarrow n\pi^0\eta). \quad (11)$$

Inserting Eq. (1) into Eq. (11), one sees that in the coherent process of Eq. (10) the isoscalar excitation of  $N^*$  resonances is forbidden, so that only the isovector part of the  $\gamma N \rightarrow N^*$  transition and  $I = 3/2$  resonances can contribute. Thus the coherent reaction works as an isospin filter. In Fig. 6(f), the data are compared to the model predictions from Ref. [46], where the elementary production operator from [23] (Solution(I)) was used. As mentioned above, the model [46] contains only the  $\Delta$ -like  $I = 3/2$  resonances as initial states, and the  $I = 1/2$  amplitude, coming only from the Born terms, is insignificant. Therefore, the good agreement between data and the predictions in Fig. 6(f) is further evidence that the isospin decomposition is understood and that excitation of  $N^*$  resonances in the initial state of this reaction should not be significant.

It should be mentioned that contrary to single  $\eta$  production, coherent production of  $\eta\pi$  pairs is allowed for spin/isospin zero nuclei such as  $^4\text{He}$ . This reaction could thus be used [25] for the search for  $\eta$ -mesic  $^4\text{He}$  similar to the use of  $\eta$  production for  $\eta$ -mesic  $^3\text{He}$  [33,48].

For the quasi-free  $\gamma N \rightarrow N\pi^0\eta$  and  $\gamma N \rightarrow N'\pi^\pm\eta$  reactions, angular distributions, invariant mass distributions, and the helicity asymmetries  $I^\odot$  have been analyzed. All differential spectra are shown for the  $W$  ranges 1700 - 1750 MeV, 1750 - 1800 MeV, 1800 - 1850 MeV, and 1850 - 1900 MeV.

The distributions of the cm polar angles of the  $\eta$ -meson are summarized in Fig. 7. For these spectra (and also for all following differential spectra), one should note that in

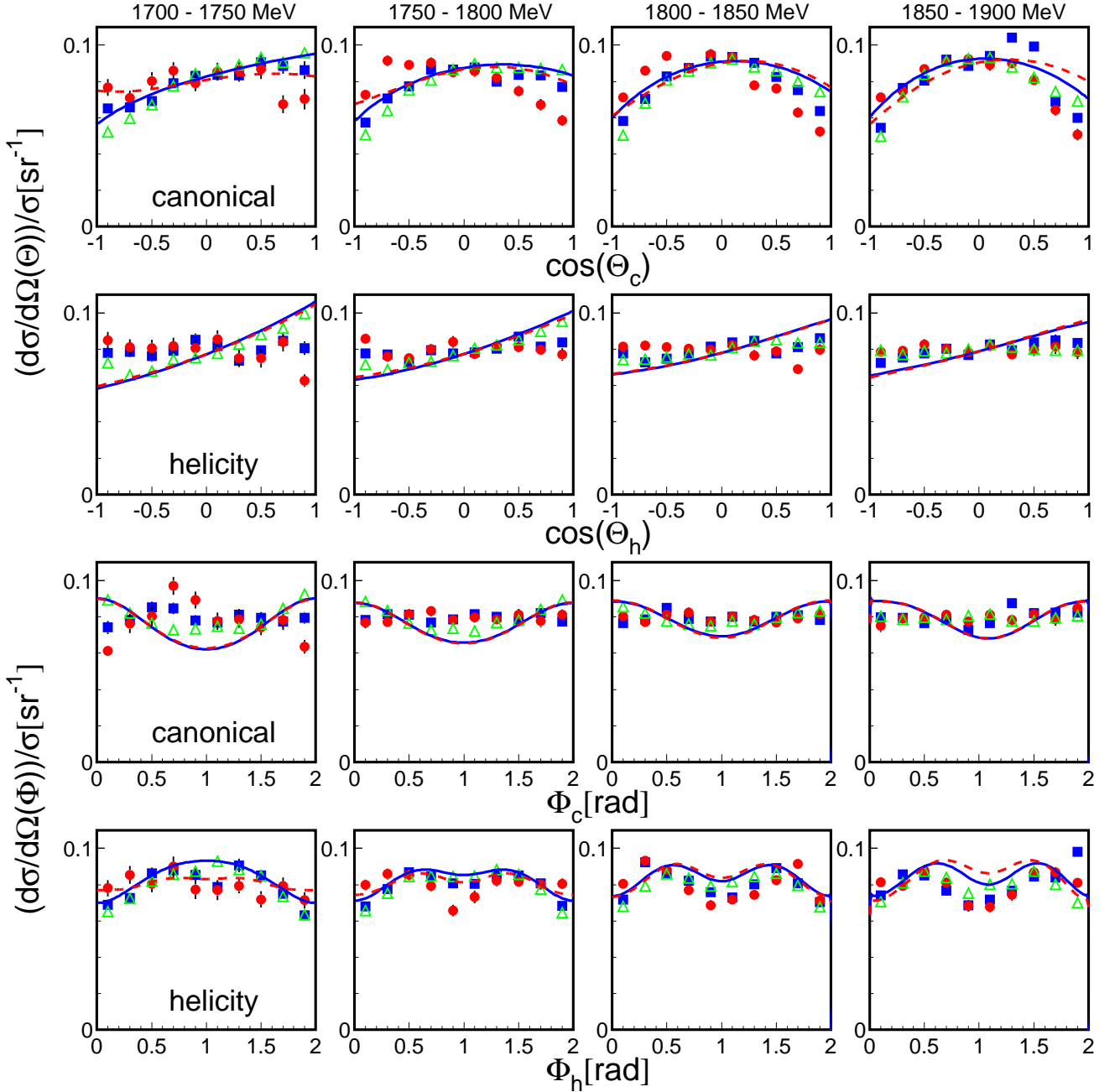


**Fig. 8.** Angular distributions of the  $\pi^0$  mesons from the  $\gamma N \rightarrow N\eta\pi^0$  reactions in the frames defined in Fig. 1 for different energy bins (given at top of the figure).  $\Theta_c$ ,  $\Phi_c$  ( $\Theta_h$ ,  $\Phi_h$ ) are the polar and azimuthal angles in the canonical and helicity frames (Fig. 1), respectively. Notation for the experimental data same as in Fig. 7. Curves for model results from [23], solid (blue) for target protons, dashed (red) target neutrons (predictions for protons and neutrons almost identical for most figures). Only the statistical uncertainties are shown.

general, the statistical quality of the data is not as good with charged pions in the final state as for neutral pions. This is because the total cross sections for charged pions are smaller by a factor of two and the detection efficiency for charged pions is also lower (in particular for low-energy pions). Furthermore, due to the larger detection efficiency for protons compared to neutrons (roughly a factor of three), the statistical precision for reactions involving recoil protons is better than for recoil neutrons.

Thus for reactions with neutral mesons, more precise data were obtained for target protons (free or quasi-free) than for quasi-free neutrons, for charged pions it is the opposite.

The main observations for the  $\eta$  polar angle distributions are: after renormalization by the total cross section, there are almost no differences between free and quasi-free proton data. This observation is true for almost all differential spectra and means that the FSI affects mainly the absolute scale of the cross section but has only a small

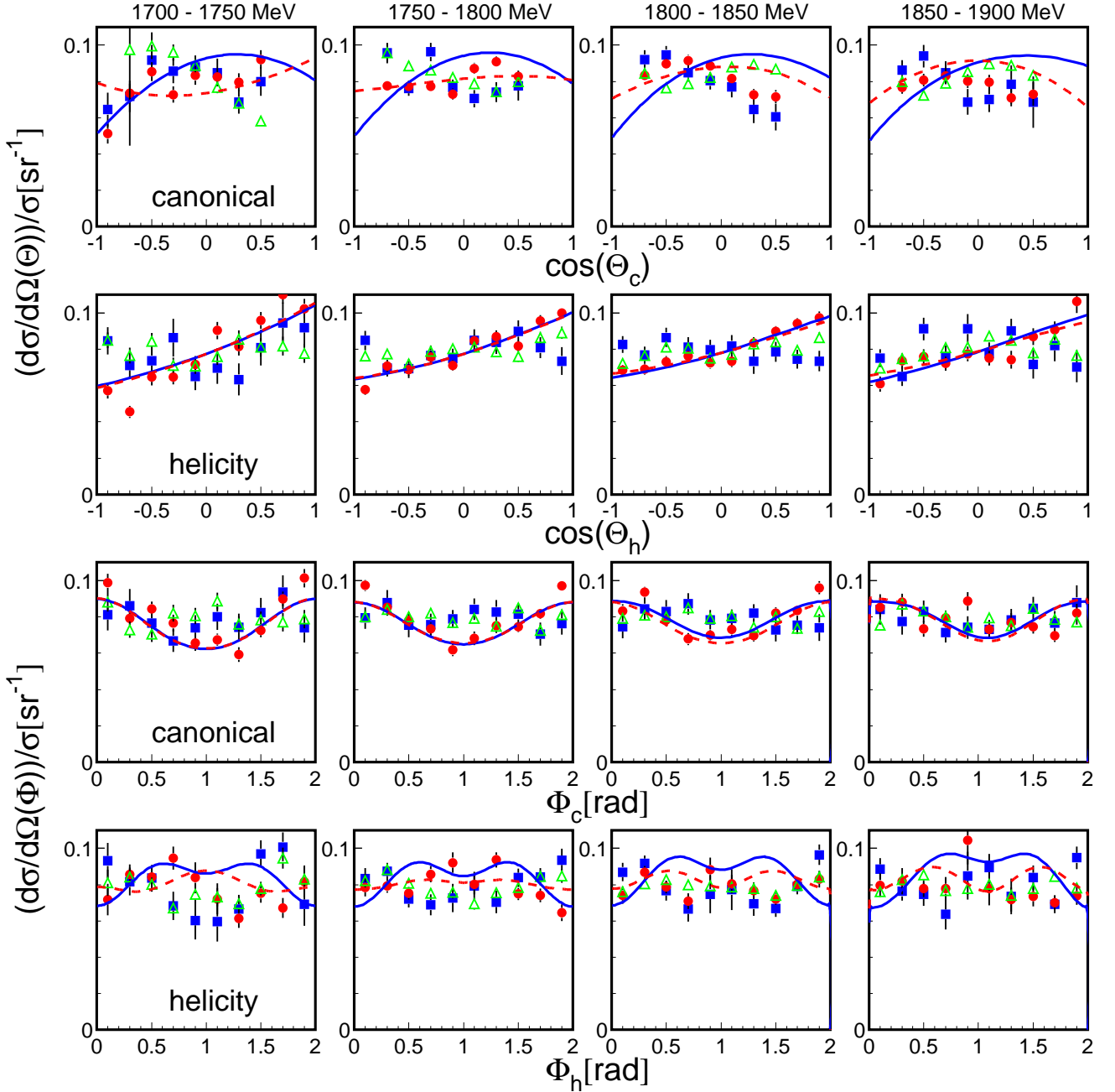


**Fig. 9.** Same as in Fig. 8 for  $\pi^\pm$  mesons from the  $\gamma N \rightarrow N \eta \pi^\pm$  reactions.

effect on the shape of the spectra. As expected, the results for target neutrons and protons are similar because of the dominant excitation of  $\Delta^*$ -resonances as doorway states. For the same reason, reactions with neutral and charged pions in the final state are also identical within uncertainties.

The distributions are in good agreement in all isospin channels (three of which have been measured for the first time) with the model predictions from [23] assuming dominance of the  $\Delta(1700)3/2^- \rightarrow \Delta(1232)3/2^+$  decay in the threshold region and, at higher photon energies, of the  $\Delta(1940)3/2^- \rightarrow \Delta(1232)3/2^+$  decay. Some shape deviations between predictions and measured data

appear only for charged pions at lowest and highest incident photon energies. The predicted distributions are almost isotropic close to threshold where the  $s$ -wave decay of the  $\Delta(1700)3/2^-$  to the  $\Delta(1232)\eta$  intermediate state dominates. At higher photon energies the decay of this state to  $\Delta(1232)\eta$  in relative  $d$ -wave and contributions from further initial  $\Delta$  states may also become significant, in particular in interference terms. In solution (I) from [23], in addition to  $\Delta(1700)3/2^-$ , the  $\Delta(1940)3/2^-$  state makes an important contribution. Further small contributions arise from the  $\Delta(1905)5/2^+$  and  $\Delta(1920)3/2^+$  resonances, while the  $d$ -wave decay of the  $\Delta(1700)3/2^-$  and nucleon Born terms play almost no role.

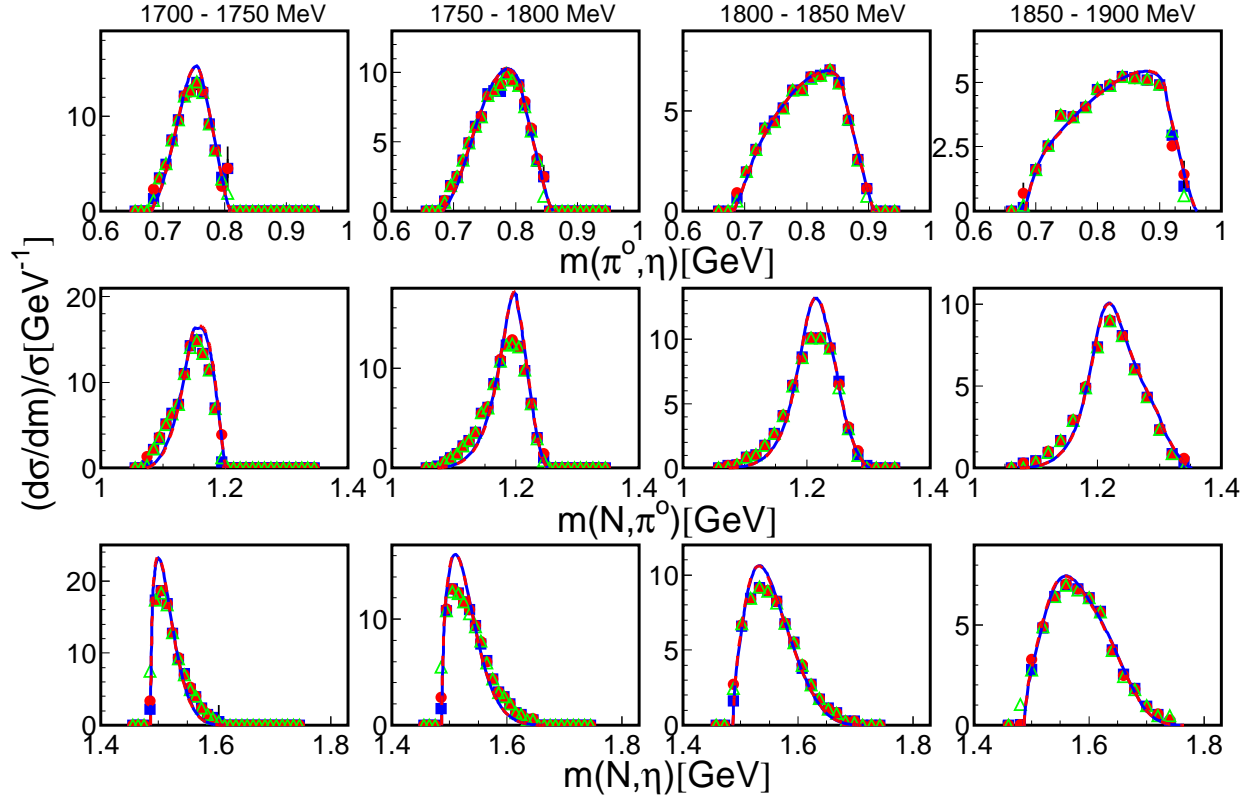


**Fig. 10.** Invariant mass distributions for the  $\pi^0\eta N$  final state. Notation is the same as in Fig. 7. Model predictions from [23] are almost identical for target protons (blue, solid) and neutrons (dashed, red). Only the statistical uncertainties are shown. Upper row:  $\eta$  - pion invariant masses, central row: nucleon - pion, bottom row: nucleon -  $\eta$ .

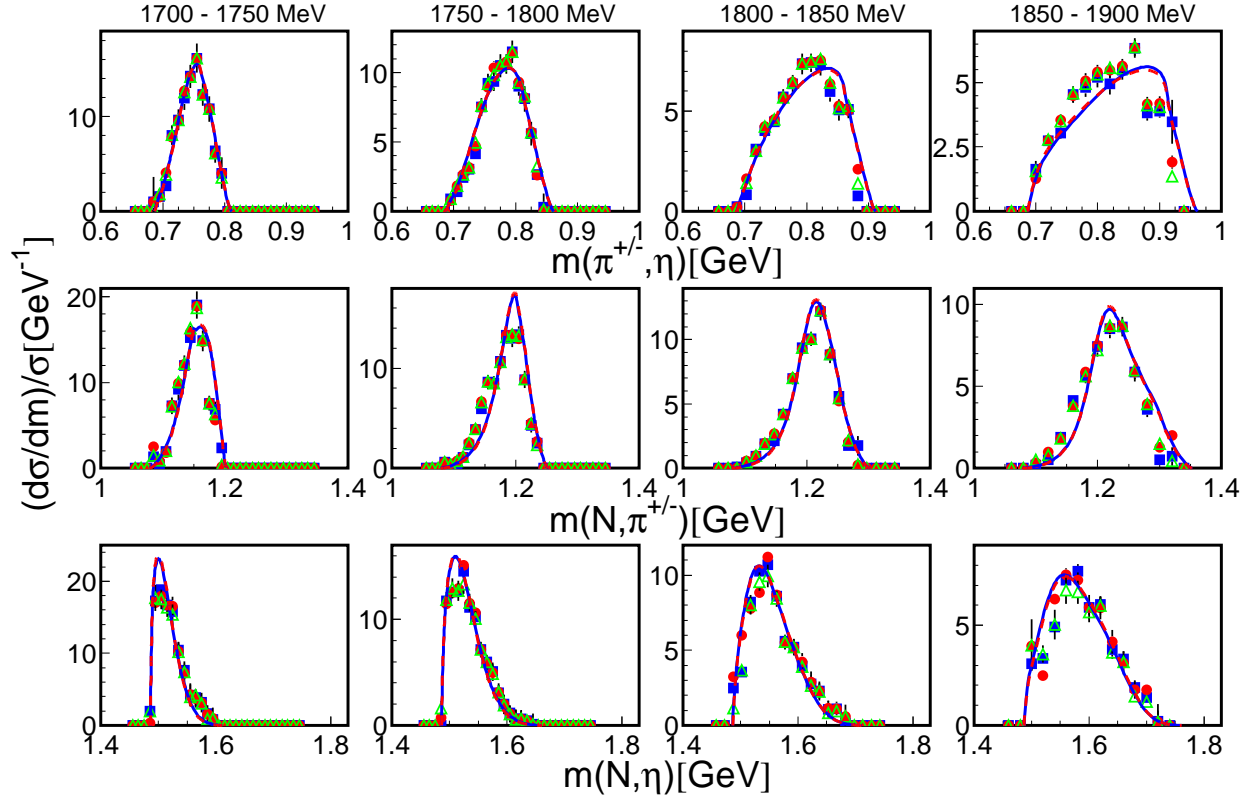


**Fig. 11.** Invariant mass distributions for the  $\pi^\pm\eta N$  final state. Upper row:  $\eta$  - pion invariant mass, central row: nucleon - pion, bottom row: nucleon -  $\eta$ . Notation is the same as in Fig. 7.

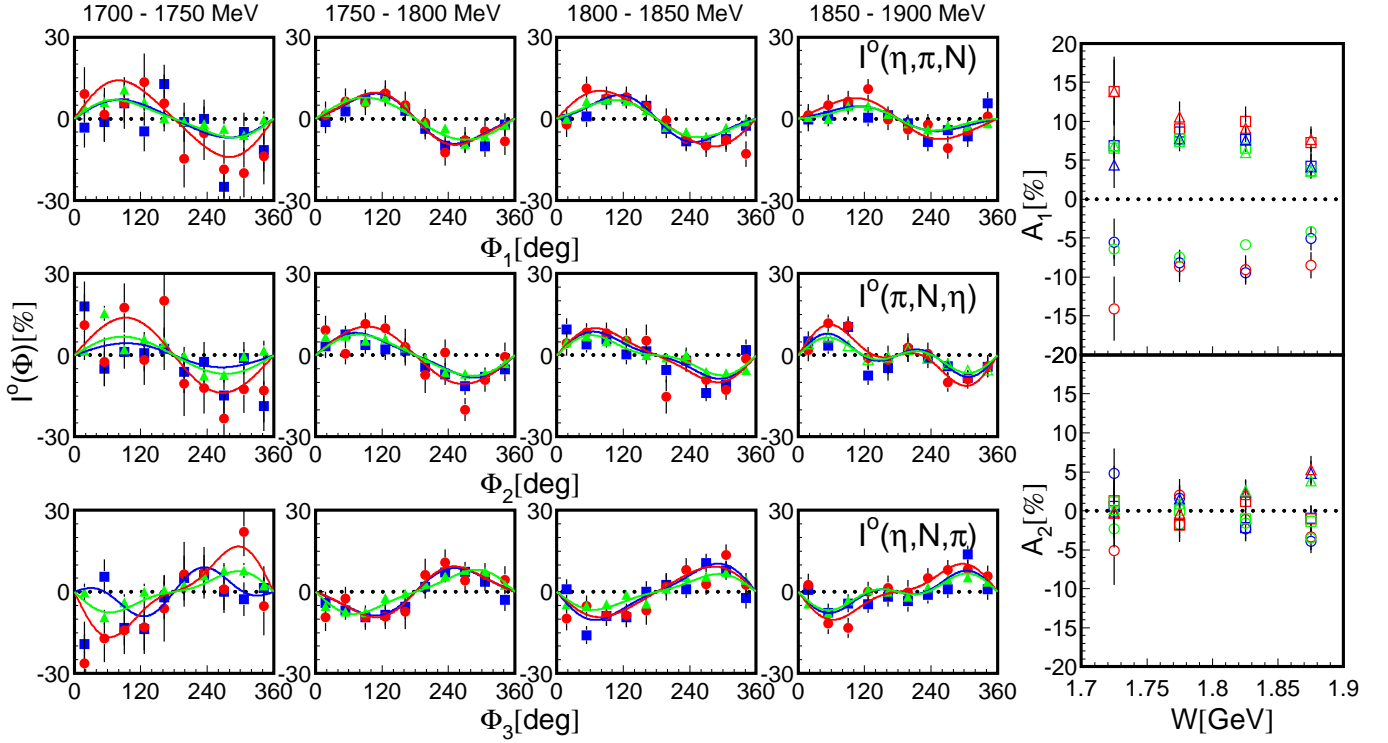


**Fig. 12.** Left hand side: Beam-helicity asymmetries  $I^\circ(\Phi)$  for the reactions  $\gamma N \rightarrow N\pi^0\eta$  for different  $W$  ranges given at top of Fig. The three rows correspond to the asymmetries  $I^\circ(\eta, \pi, N)$ ,  $I^\circ(\pi, N, \eta)$ , and  $I^\circ(\eta, N, \pi)$  defined in Sec. 2. (Green) triangles: free protons in initial state, (blue) squares: quasi-free protons, (red) circles: quasi-free neutrons. Solid curves: fits to data with Eq. 6 (same color code as for data). Panel at right hand side: fit coefficients  $A_1$  and  $A_2$  as defined in Eq. (6). Colors indicate reaction type like above, open squares:  $I^\circ(\eta, \pi, N)$ , open triangles:  $I^\circ(\pi, N, \eta)$ , open circles:  $I^\circ(\eta, N, \pi)$ .

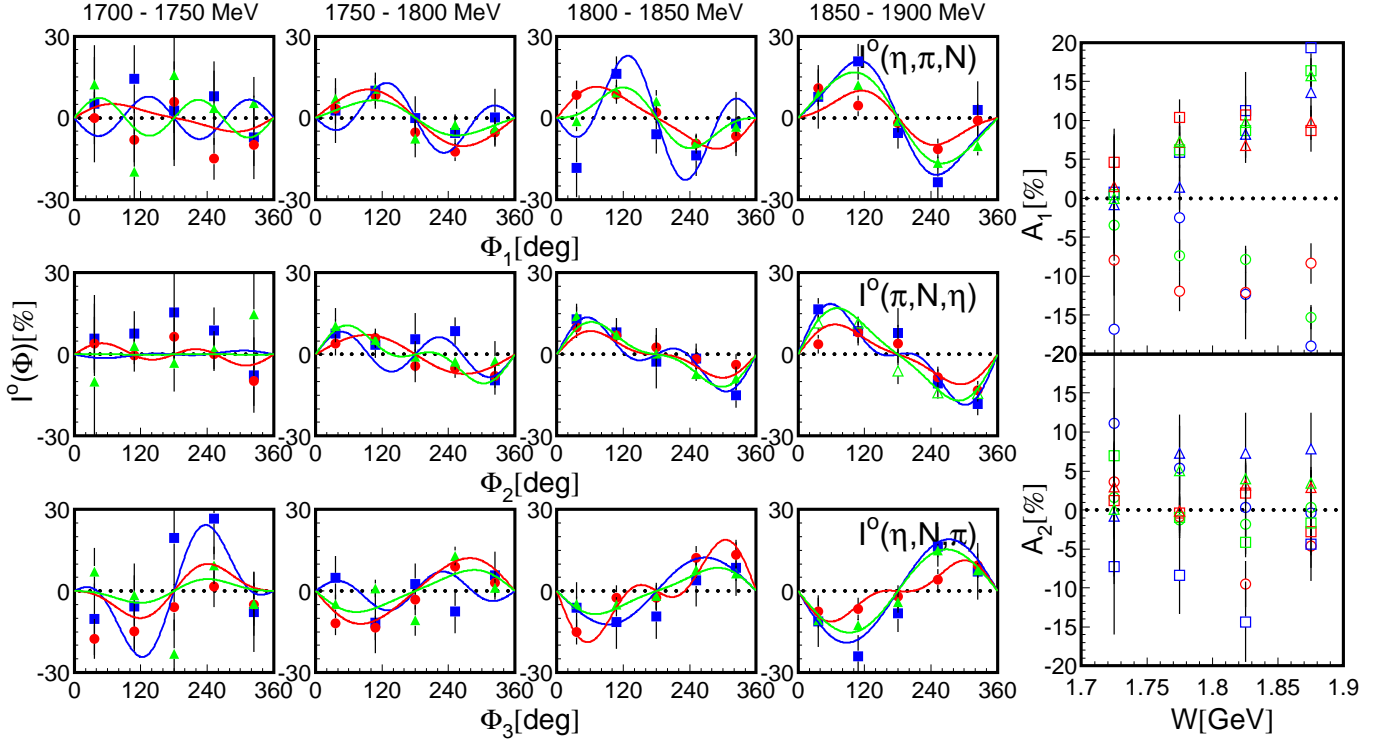


**Fig. 13.** Same as Fig. 12 for charged pions.

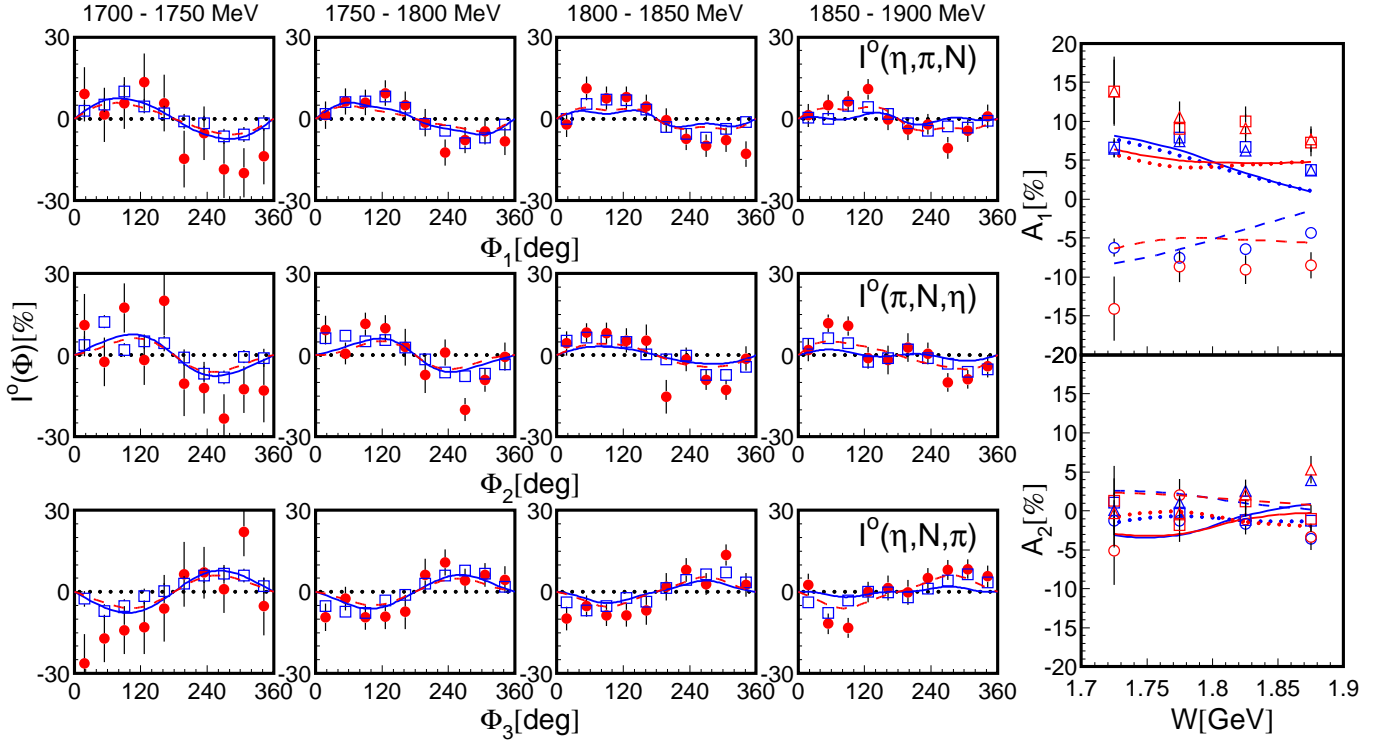


**Fig. 14.** Beam-helicity asymmetries for the reactions  $\gamma N \rightarrow N\pi^0\eta$  compared to predictions from Ref. [23]. (Blue) open squares: average of free and quasi-free proton data shown in Fig. 12, (red) circles: quasi-free neutrons (same data as in Fig. 12). Curves: model predictions from [23], solid (blue): proton target, dashed (red) neutron target. Panel at right hand side: fit coefficients  $A_1$  and  $A_2$ . Colors indicate reaction type like above, open squares:  $I^\circ(\eta, \pi, N)$ , open triangles:  $I^\circ(\pi, N, \eta)$ , open circles:  $I^\circ(\eta, N, \pi)$ . Curves: model predictions from [23]; blue (red) for proton (neutron) target; solid, dashed, dotted for  $I^\circ(\eta, \pi^0, p)$ ,  $I^\circ(\eta, N, \pi)$ ,  $I^\circ(\pi, N, \eta)$ .

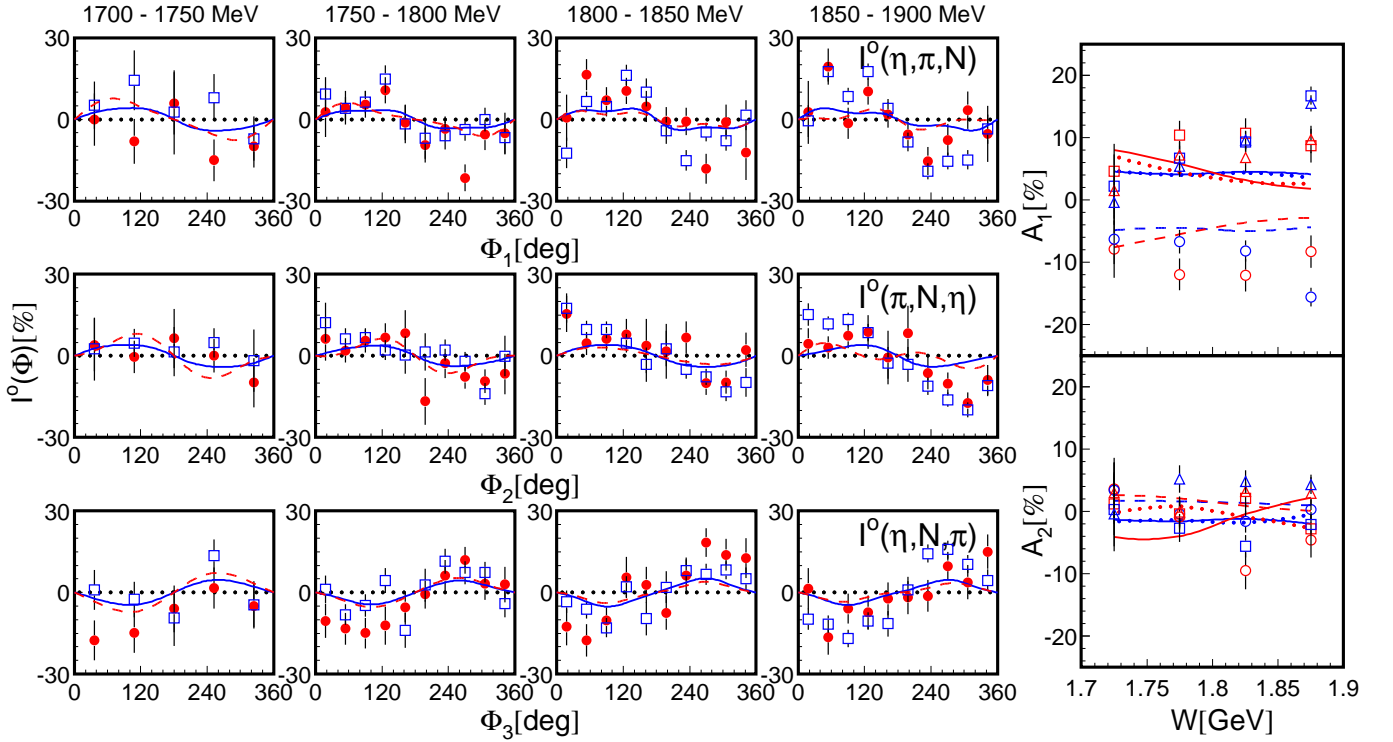


**Fig. 15.** Same as Fig. 14 for charged pions.



Angular distributions of the pions in the canonical and helicity frames (see Sec. 2 for definitions) for the reactions with neutral pions are summarized in Fig. 8 and for charged pions in Fig. 9. Similar observations as for the  $\eta$  polar-angle distributions can be made. In general, the free and quasi-free proton data are quite similar, indicating only small FSI effects on the shape of the angular distributions. The measured angular distributions show only small variations between different target nucleons and the charge type of the final state pions and are in overall fair agreement with the model predictions.

Invariant mass distributions of the meson-meson and meson-nucleon pairs are shown in Figs. 10 and 11. These data are in almost perfect agreement for free and quasi-free protons and quasi-free neutrons as targets and for final state neutral and charged pions. They agree with the model predictions from [23] which are also essentially identical for all reaction channels.

Some deviations between experimental data and predictions occur in the peaks of the narrow distributions, but this may be caused partly by experimental resolution effects, which have not been folded into the model predictions. The shapes of the invariant mass distributions are dominated by the sequential  $\Delta^* \rightarrow \Delta\eta \rightarrow N\eta\pi$  decay chain. All reactions show a pronounced peak in the  $N\pi$  invariant mass from the intermediate  $\Delta(1232)$  state (for the lowest photon energies the intermediate  $\Delta(1232)$  can be only populated at invariant masses below its peak value). There are no particular structures from the  $N(1535)1/2^- \pi$  intermediate state visible in the  $N\eta$  invariant mass distributions. In previous measurements of the  $\gamma p \rightarrow p\pi^0\eta$  reaction [20], such contributions only became prominent at higher photon energies. They are expected close to the lower phase-space limit of the distributions where they are difficult to identify (see, however, the discussion below of the asymmetries which show more evidence for such contributions). The  $\pi\eta$  invariant masses are also structureless because the  $a_0$  meson with its strong decay to  $\pi\eta$  has a mass of 980 MeV and lies thus outside the range of the current measurements.

Finally, the beam-helicity asymmetries introduced in Sec. 2 have been analyzed. The results are shown in Figs. 12 and 13. They have been fitted with the expansion from Eq. 6 and the fit results for the expansion coefficients are also shown. This type of asymmetry is usually very sensitive to small reaction amplitudes such as from background terms (see e.g. [5,8,9] for similar results for pion pairs). Again, the comparison of free and quasi-free proton results indicates no significant FSI effects on this observable. The results for target protons and neutrons are similar for all three asymmetries over the entire investigated energy range. The comparison of the reactions with neutral and charged pions is not so stringent due to the rather poor statistical quality of the data for charged pions, but qualitatively, those data are also quite similar. As already reported in [22] for  $I^\odot(\pi^0, p, \eta)$ , only the  $A_1$  coefficient is significantly different from zero. The  $A_1$  magnitude is similar for reactions with charged and neutral pions. There are suggestions in the data of small differences in the energy

dependence of the beam helicity asymmetries for charged and neutral pions, although the statistical uncertainties are large, particularly for charged pions at low energies.

The results are compared in Figs. 14 and 15 to the predictions from Ref. [23]. One should note that these model results are really predictions, as previously only a few results for  $I^\odot(\pi^0, p, \eta)$  reported in [22] were available. Data for the other isospin channels and the other types of asymmetry have been measured here for the first time and were not included in the model fits. For simplification of the figures and for better statistical quality, the experimental results for free and quasi-free proton targets have been averaged (the comparison in Figs. 12 and 13 did not reveal any systematic differences). The agreement between experimental data and model predictions is quite good. As long as the  $3/2^-$  wave dominates, the  $A_1$  coefficient comes from the interference of the  $\eta\Delta(1232)$  and  $\pi N(1535)$  decay modes of the two  $3/2^-$  resonances  $\Delta(1700)$  and  $\Delta(1940)$ . Therefore, the observed behavior is evidence for contributions from the  $\pi N(1535)$  intermediate state, which is difficult to establish in the invariant mass distributions. Other resonances and background mechanisms mostly contribute to higher order terms in Eq. 6 (which are almost insignificant in the experimental results within the achieved statistical accuracy). In particular, as discussed in [22], the coefficient  $A_2$  is due to interference of the positive parity states with the dominant  $3/2^-$  wave.

## 6 Summary and Conclusions

Photoproduction of  $\pi\eta$  pairs off nucleons has been studied for all possible isospin channels using a liquid deuterium target (i.e. with quasi-free nucleons bound in the deuteron) and, for comparison, for the reactions  $\gamma p \rightarrow p\eta\pi^0$  and  $\gamma p \rightarrow n\eta\pi^+$ , with a free proton target (liquid hydrogen). For all reactions, total cross sections, various angular distributions, invariant mass distributions of meson-meson and meson-nucleon pairs, and all possible types of beam-helicity asymmetries (circularly polarized photon beam) have been measured. For the quasi-free measurements, the effects from Fermi motion have been eliminated by a full kinematic reconstruction of the final state.

The major findings are the following: the absolute scale of the cross sections for free and quasi-free protons is different. Total cross sections for production of  $\pi^0\eta$  pairs off protons bound in the deuteron are suppressed with respect to the free proton to roughly 75%. For protons bound in  $^3\text{He}$  nuclei, the reduction is to 60%. This is a clear indication of FSI effects, which are larger for the more strongly bound helium nucleus. As in the case for reactions with single pion production, FSI effects are smaller for final states with charged pions (reduced to 90% for protons bound in the deuteron). This is most likely due to the different FSI in the  $nn$  and  $pp$  systems compared to the  $np$  system, but there is so far no quantitative modeling of these FSI effects. The measured asymmetries show no significant differences between free and quasi-free protons and also the angular and invariant-mass distributions agree quite well after renormalization to the scale of the

total cross sections. Thus one can conclude that the FSI effects influence mainly the absolute scale of the cross sections, but are not so important for polarization observables and for shapes of differential cross sections (the same observation has previously been made for photoproduction of pion pairs [8,9,13]).

The ratios of the total cross sections for the different isospin channels are all in good agreement with Eq. 2 which was derived under the assumption of a dominant  $\gamma N \rightarrow \Delta^* \rightarrow \Delta(1232)\eta \rightarrow N\eta\pi$  reaction chain. Apart from the FSI related effects noted in the absolute cross sections, all differential cross sections agree quite well with a simple isobar model [23] based on a dominant contribution from the above reaction with  $\Delta^* = \Delta 3/2^-$  ( $\Delta(1700)$  at threshold,  $\Delta(1940)$  at higher energies). The beam-helicity asymmetries are naturally explained in the framework of this model when interferences between the decays of the  $\Delta^* 3/2^-$  states to the  $\eta\Delta(1232)3/2^+$  and  $\pi N(1535)1/2^-$  final states are considered. In addition, small contributions from a few further  $\Delta$  resonances (which manifest themselves mainly in angular distributions), very minor contributions from nucleon Born terms, and no contributions at all from isospin  $I = 1/2$   $N^*$  resonances are required in the model. The latter would destroy the simple Clebsch-Gordan coefficient relation from Eq. 2 due to the different photo-couplings of  $N^*$  resonances for protons and neutrons. This special situation has made it possible to make good model predictions for all isospin channels based on experimental results for the  $\gamma p \rightarrow p\eta\pi^0$  reaction. This is very different from single  $\eta$  or single  $\pi$  photoproduction. In the latter case abundant results for different observables for three of the four possible isospin channels were available ( $\gamma p \rightarrow p\pi^0$ ,  $\gamma p \rightarrow n\pi^+$ ,  $\gamma n \rightarrow p\pi^-$ ). Since there are only three independent isospin amplitudes, (as in Eq. 1) this should be enough to predict the results for the fourth channel ( $\gamma n \rightarrow n\pi^0$ ). However, results from different models do not agree and none of them predicted correctly the recently reported experimental data [32] for the fourth reaction.

Photoproduction of  $\pi\eta$  pairs is an efficient tool for the study of  $\Delta$  excitations at moderate energies, in particular for the  $\Delta(1700)3/2^-$ . This reaction will most likely become a similar benchmark for this state as single  $\eta$  production is for the  $N(1535)1/2^-$  [49,50]. It seems that already now at the current energies, production of  $\eta\pi$  pairs is much better understood than production of pion pairs, for which results from different models vary strongly and are not in good agreement with experimental data [13].

### Acknowledgments

We wish to acknowledge the outstanding support of the accelerator group and operators of MAMI. This work was supported by Schweizerischer Nationalfonds (200020-156983, 132799, 121781, 117601, 113511), Deutsche Forschungsgemeinschaft (SFB 443), the INFN-Italy, the European Community-Research Infrastructure Activity under FP7 programme (Hadron Physics2, grant agreement No. 227431), the UK Science and Technology Facilities

Council (ST/J000175/1, ST/G008604/1, ST/G008582/1, ST/J00006X/1), the Natural Sciences and Engineering Research Council (NSERC, FRN: SAPPJ-2015-00023), Canada. This material is based upon work also supported by the U.S. Department of Energy, Office of Science, Office of Nuclear Physics Research Division, under Award Numbers DE-FG02-99-ER41110, DE-FG02-88ER40415, and DE-FG02-01-ER41194 and by the National Science Foundation, under Grant Nos. PHY-1039130 and IIA-1358175. A. Fix acknowledges support from the MSE program Nauka (Project 3.825.2014/K). We thank the undergraduate students of Mount Allison University and The George Washington University for their assistance.

### References

1. W.T. Chiang and F. Tabakin, Phys. Rev. C **55**, 2054 (1997).
2. W. Roberts and T. Oed, Phys. Rev. C **71**, 055201 (2005).
3. A.V. Sarantsev *et al.*, Phys. Lett. B **659**, 94 (2008).
4. U. Thoma *et al.*, Phys. Lett. B **659**, 87 (2008).
5. D. Krambrich *et al.*, Phys. Rev. Lett. **103**, 052002 (2009).
6. V.L. Kashevarov *et al.*, Phys. Rev. C **85**, 064610 (2012).
7. F. Zehr *et al.*, Eur. Phys. J. A **48**, 98 (2012).
8. M. Oberle *et al.*, Phys. Lett. B **721**, 237 (2013).
9. M. Oberle *et al.*, Eur. Phys. J. A **50**, 54 (2014).
10. A. Thiel *et al.*, Phys. Rev. Lett. **114**, 091803 (2015).
11. V. Sokhoyan *et al.*, Phys. Lett. B **746**, 127 (2015).
12. V. Sokhoyan *et al.*, Eur. Phys. J. A **51**, 95 (2015).
13. M. Dieterle *et al.*, Eur. Phys. J. A **51**, 142 (2015).
14. T. Nakabayashi *et al.*, Phys. Rev. C **74**, 035202 (2006).
15. J. Ajaka *et al.*, Phys. Rev. Lett. **100**, 052003 (2008).
16. I. Horn *et al.*, Phys. Rev. Lett. **101**, 202002 (2008).
17. I. Horn *et al.*, Eur. Phys. J. A **38**, 173 (2008).
18. E. Gutz *et al.*, Eur. Phys. J. A **35**, 291 (2008).
19. E. Gutz *et al.*, Phys. Lett. B **687**, 11 (2010).
20. E. Gutz *et al.*, Eur. Phys. J. A **50**, 74 (2014).
21. V. Kashevarov *et al.*, Eur. Phys. J. A **42**, 141 (2009).
22. V. Kashevarov *et al.*, Phys. Lett. B **693**, 551 (2010).
23. A. Fix, V.L. Kashevarov, A. Lee, and M. Ostrick, Phys. Rev. C **82**, 035207 (2010), and priv. com.
24. A. Fix and H. Arenhövel, Phys. Rev. C **83**, 015503 (2011).
25. B. Krusche and C. Wilkin, Prog. Part. Nucl. Phys. **80**, 43 (2015).
26. M. Döring, E. Oset, D. Strottman, Phys. Lett. B **639**, 59 (2006).
27. M. Döring, E. Oset, D. Strottman, Phys. Rev. C **73**, 045209 (2006).
28. A. Käser *et al.*, Phys. Lett. B **748**, 244 (2015).
29. B. Krusche, Eur. Phys. J. Special Topics **198**, 199 (2011).
30. D. Werthmüller *et al.*, Phys. Rev. Lett. **111**, 232001 (2013).
31. D. Werthmüller *et al.*, Phys. Rev. C **90**, 015205 (2014).
32. M. Dieterle *et al.*, Phys. Rev. Lett. **112**, 142001 (2014).
33. F. Pheron *et al.*, Phys. Lett. B **709**, 21 (2012).
34. L. Witthauer *et al.*, Eur. Phys. J. A **49**, 154 (2013).
35. H. Herminghaus *et al.*, IEEE Trans. on Nucl. Science. **30**, 3274 (1983).
36. Th. Walcher, Prog. Part. Nucl. Phys. **24**, 189 (1990).
37. I. Anthony *et al.*, Nucl. Inst. and Meth. A **301**, 230 (1991).

- 38. S.J. Hall, G.J. Miller, R. Beck, P.Jennewein, Nucl. Inst. and Meth. A **368**, 698 (1996).
- 39. J.C. McGeorge *et al.*, Eur. Phys. J. A **37**, 129 (2008).
- 40. H. Olsen and L.C. Maximon, Phys. Rev. **114**, 887 (1959).
- 41. R. Novotny, IEEE Trans. Nucl. Sci. **38**, 379 (1991).
- 42. A.R. Gabler *et al.*, Nucl. Inst. and Meth. A **346**, 168 (1994).
- 43. A. Starostin *et al.*, Phys. Rev. C **64**, 055205 (2001).
- 44. D. Watts, in *Calorimetry in Particle Physics, Proceedings of the 11th International Conference, Perugia, Italy 2004*, edited by C. Cecchi, P. Cenci, P. Lubrano, and M. Pepe (World Scientific, Singapore, 2005, p. 560).
- 45. S. Agostinelli *et al.*, Nucl. Instr. Meth. A **506**, 250 (2003).
- 46. M. Egorov and A. Fix, Phys. Rev. C **88**, 054611 (2013).
- 47. B. Krusche and S. Schadmand, Prog. Part. Nucl. Phys. **51**, 399 (2003).
- 48. M. Pfeiffer *et al.*, Phys. Rev. Lett. **92**, 252001 (2004).
- 49. B. Krusche *et al.*, Phys. Rev. Lett. **74**, 3736 (1995).
- 50. B. Krusche *et al.*, Phys. Lett. B **397**, 171 (1997).